Nonclassical Velocity Statistics in a Turbulent Atomic Bose-Einstein Condensate

A. C. White,* C. F. Barenghi, N. P. Proukakis, A. J. Youd, and D. H. Wacks

School of Mathematics and Statistics, Newcastle University, Newcastle upon Tyne, NE1 7RU, United Kingdom

(Received 21 August 2009; revised manuscript received 26 January 2010; published 17 February 2010)

In a recent experiment Paoletti *et al.* [Phys. Rev. Lett. **101**, 154501 (2008)] monitored the motion of tracer particles in turbulent superfluid helium and inferred that the velocity components do not obey the Gaussian statistics observed in ordinary turbulence. Motivated by their experiment, we create a small 3D turbulent state in an atomic Bose-Einstein condensate, compute directly the velocity field, and find similar nonclassical power-law tails. We obtain similar results in 2D trapped and 3D homogeneous condensates, and in classical 2D vortex points systems. This suggests that non-Gaussian turbulent velocity statistics describe a fundamental property of quantum turbulence. We also track the decay of the vortex tangle in the presence of the thermal cloud.

DOI: 10.1103/PhysRevLett.104.075301 PACS numbers: 67.25.dk, 03.75.Kk, 47.37.+q

Quantum turbulence (a dynamic tangle of discrete, reconnecting vortices) is studied in superfluid ^{4}He [1], ^{3}He-B [2], and, more recently, in atomic Bose—Einstein condensates (BECs) [3–5]. The defining property of these quantum fluids is that the superfluid velocity is proportional to the gradient of the phase of a complex order parameter. Therefore, whereas in classical ordinary fluids (such as air or water) the rotational motion is unconstrained, in a quantum fluid the vorticity is singular: the velocity magnitude, at distance r from the axis of a quantum vortex, is $\kappa/(2\pi r)$, κ being the quantum of circulation.

Recent work has revealed remarkable similarities [6] between classical turbulence and quantum turbulence (the same Kolmogorov energy spectrum [7], temporal vorticity decay [8], pressure drops in pipes and channels [9], and drag crisis behind a sphere [10]). In a recent experiment in superfluid ^{4}He Paoletti *et al.* [11] have identified an important dissimilarity: the components of the turbulent velocity field do not obey the usual Gaussian distribution which is observed in ordinary turbulence [12], but follow power-law-like behavior.

The main aim of this Letter is to remark that non-Gaussian velocity statistics are a fundamental property of turbulence in a quantum fluid. To achieve this aim, we move from ^{4}He to atomic BECs. The agreement with the experiment that we find suggests that power–law behavior is indeed typical of quantum turbulence, in stark contrast with classical turbulence.

To create a vortex tangle in a confined BEC we choose the technique of phase imprinting [13]; although this is not the only method to generate turbulence [5,14,15], it is specific to BECs, and can in principle be exploited to create isotropic or polarized tangles. We study the decay of the tangle by evolving the three-dimensional (3D) Gross-Pitaevskii equation (GPE) for realistic experimental parameters, and discuss the effect of the thermal cloud. An ultracold dilute atomic gas confined in a spherical trap is described by the dimensionless GPE

$$i\frac{\partial}{\partial t}\psi = \left(-\frac{1}{2}\nabla^2 + \frac{1}{2}\mathbf{r}^2 + C|\psi|^2\right)\psi, \qquad (1)$$

for the complex wave function Ψ, where $\mathbf{r}$ is the position vector; $\psi = a_0^{3/2}N^{-1/2}\Psi$ is dimensionless and satisfies the constraint $\int d\mathbf{r}|\psi|^2 = 1$. In writing Eq. (1) we use the harmonic oscillator length $a_0 = \sqrt{\hbar/(m\omega)}$ as unit of distance and the inverse trapping frequency $1/\omega$ as unit of time, where m is the mass of one atom, $C = 4\pi Na/a_0$ is the dimensionless measure of the interaction between bosons, N is the number of atoms and a is the scattering length. Finite temperature effects are qualitatively simulated by replacing i at the left-hand side of Eq. (1) with $(i - \gamma)$ [16] where γ models the dissipation due to the thermal cloud as justified by more involved treatments [17].

We employ realistic experimental parameters for a ^{23}Na condensate ($a = 2.75$ nm) of $N = 10^5$ atoms and trapping frequency $\omega = 2\pi \times 150$ Hz, giving $C = 2.019 \times 10^3$, $a_o = 1.71$ μm and 1.06 ms as time unit. In a homogeneous condensate the healing length ξ is estimated by balancing the kinetic energy per particle and the interaction strength, which implies the (dimensionless) $\xi = (2Cn)^{-1/2}$ where $n = |\psi|^2$ is the density. In a harmonic trap, n is position dependent, so we estimate ξ from the mean density; for example, at $t = t_0$ (Fig. 1), $\langle n\rangle = 1.35 \times 10^{-3}$ and $\langle\xi\rangle = 0.43$.

Equation (1) is evolved pseudospectrally via XMDS [18] in 3D using a 4th order Runge-Kutta method and periodic boundary conditions. The spatial domain $|x|$, $|y|$, $|z| \leq 8$ is discretized on a 128^3 grid with time step $\Delta t = 10^{-4}$. We have verified that the results are independent of spatial and temporal stepsize.

The initial condition is created by phase-imprinting a grid of 17 vortices oriented parallel to the Cartesian axes in a staggered way (no vortices intersect), and propagating this configuration for a short period in imaginary time (which is equivalent to replacing t by $-it$ in Eq. (1)) while continuously renormalizing ψ, until the density adjusts to

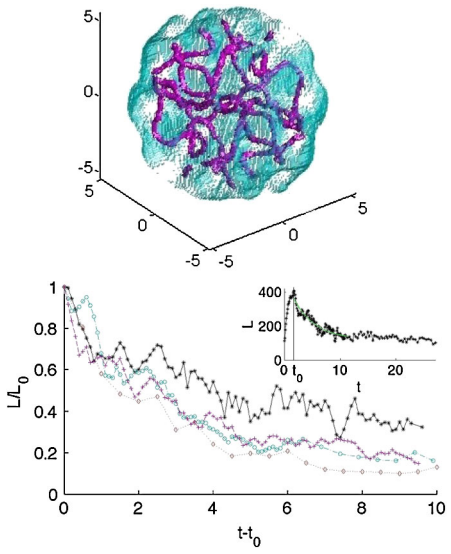

FIG. 1 (color online). (Top): 3D turbulent state within the condensate edge (blue shading) at $t_0 = 1.9$ and $\gamma = 0$; the maximum density (used to determine the condensate edge) is $n = 4.39 \times 10^{-3}$. (Bottom) Evolution of normalized total length $L(t - t_0)/L_0$ for $\gamma = 0$ (black asterisks), 0.015 (purple pluses), 0.03 (blue circles, ○), and 0.06 (red diamonds) corresponding to the same initial state; the inset shows the initial increase of $L(t)$ for $t < t_0$ and the exponential fit for $\gamma = 0$ (solid green line).

reveal the desired vortex structure. This is then propagated in real time. Initially the vortices reconnect and become excited, resulting in an increase in the total vortex line length $L(t)$. This increase continues up to some time t_0, when $L(t)$ achieves its peak value L_0, and a maximally tangled turbulent state has been generated [Fig. 1(top)]. At this point the dimensionless vortex line density (vortex length divided by volume) is 0.79. The vortex line length evolution for $t > t_0$ is shown in Fig. 1(bottom). Since no energy is injected the turbulence is not sustained but decays over a time of the order $t \approx 10$, as vortices reconnect, break up and decay into sound waves [19], or leave the condensate. Our calculation lasts longer (up to $t = 27$) at which time one long vortex is left at the center of the condensate and some shorter vortices surround it closer to the condensate's edge. Large volume oscillations of the condensate at $1/3$ of the trap frequency are observed. Although the amplitude of these oscillations decreases as the turbulence decays, a method of exciting turbulence without volume oscillations would be preferable for experiments.

At each t we attribute a vortex core length to every point in the condensate at which the real and imaginary parts of ψ crosses zero (therefore defining the vortex axis) [20]. The total vortex length $L(t)$ is the sum of all identified vortex points within the condensate edge, which, throughout this work, is defined as the outermost points at which n drops below 25% of the maximum density. To compare results at different γ we fit the decay of the vortex length with the exponential form $L(t - t_0)/L_0 \sim \exp(-c(t - t_0))$ [solid line in Fig. 1 (bottom) inset], although for $\gamma = 0$ the observed decay is also consistent with $1/L(t - t_0) \propto t - t_0$ as found in [1]. Fitting over the main decay period (10 time units), yields consistent values for different grid sizes ($c = 0.151 \pm 0.005$ and 0.144 ± 0.007 for grid sizes of 128^3 and 256^3; corresponding $L_0 = 406$ and 378). We also check that the decay of $L(t)$ is largely insensitive to the initial vortex configuration obtained by imprinting extra vortices.

To obtain a qualitative understanding of the effect of the thermal cloud, we repeat the above calculation with $\gamma = 0.015$, 0.03, and 0.06. As anticipated, the role of temperature is to induce faster decay of the turbulent state, leading, respectively, to $c = 0.252 \pm 0.007$, 0.274 ± 0.006, and 0.340 ± 0.018 (with $L_0 = 369$, 339, and 300, due to the damping in the initial period $t < t_0$).

Our next step is to analyze the turbulent (dimensionless) superfluid velocity field, which we compute directly from the definition $\mathbf{v}(\mathbf{r}) = (\psi^* \nabla \psi - \psi \nabla \psi^*)/(2i|\psi|^2)$. (the derivatives of ψ being obtained spectrally). Using the Madelung representation $\psi = \sqrt{n(\mathbf{r})} \exp[i\varphi(\mathbf{r})]$, this yields $\mathbf{v}(\mathbf{r}) = \nabla \varphi(\mathbf{r})$; i.e., the velocity depends only on the condensate phase φ. We calculate the probability density function (PDF) of each Cartesian velocity component v_i ($i = x, y, z$) for $\gamma = 0$ (see Fig. 2 top) and compare it to the form that a normalized Gaussian PDF (gPDF) of the velocity would take

$$\mathrm{gPDF}(v_i) = \frac{1}{\sigma\sqrt{2\pi}} \exp\left(\frac{-(v_i - \tilde{\mu})^2}{2\sigma^2}\right), \qquad (2)$$

where σ, σ^2, and $\tilde{\mu}$ are the standard deviation, variance,

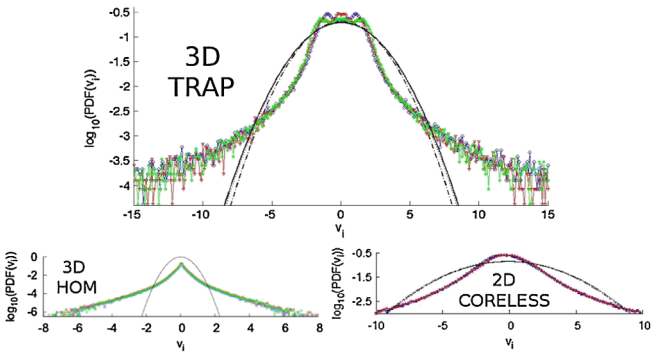

FIG. 2 (color online). Top: Trapped 3D BEC corresponding to Fig. 1 ($\gamma = 0$, $t_0 = 1.9$); $\log_{10}[\mathrm{PDF}(v_i)]$ vs velocity component v_i for v_x (blue circles, ○), v_y (red triangles, ▽), and v_z (green asterisks, *), yielding, respectively, power-law coefficients $b = -3.3$, -3.5, and -3.6. Corresponding $\log_{10}[\mathrm{gPDF}(v_i)]$ plots shown by black dotted (v_x), dash-dotted (v_y), and solid (v_z) lines, which almost overlap. The velocity components are only sampled within the condensate edge. Bottom left: $\log_{10}[\mathrm{PDF}(v_i)]$ and corresponding $\log_{10}[\mathrm{gPDF}(v_i)]$ vs v_i (symbols as above) for a 3D homogeneous condensate (average intervortex spacing $\approx 10\xi$, $b = -3.6$). Bottom right: the same for a 2D system of 50 positive and 50 negative vortex points (power law $b = -3.1$).

and mean of the data. We find that our velocity statistics are non-Gaussian and obey power-law dependence PDF(v_i) $\propto v_i^b$ with $-3.6 < b < -3.3$ in all three directions, consistently with the high-velocity tails found experimentally by Paoletti *et al.* [11] in turbulent superfluid ^{4}He (their b is -3). The non-Gaussian nature does not change if instead of the total velocity we compute the incompressible velocity [15] (thus disregarding sound modes).

We find that deviations from Gaussian behavior are less pronounced (but still noticeable) if we omit sampling the velocity very near the axis where the density is less than a prescribed cutoff. Unlike a classical vortex, there are not individually distinguishable atoms which spin about the vortex axis, and the velocity field is entirely defined by the macroscopic phase $\varphi(\mathbf{r})$ irrespective of the density $n(\mathbf{r})$, so our procedure is justified. The small wiggles in the PDF for values close to zero may be a measure of the anisotropy of the vortex tangle in our condensate and would not feature in velocity PDFs of a truly isotropic state of quantum turbulence in a larger condensate, or they could be due to the large volume oscillations of the 3D condensate.

The observed non-Gaussianity of the velocity statistics holds during the decay of the vortex tangle at different times $t = 2$ and 4 at both $\gamma = 0.03$ and $\gamma = 0.06$, suggesting that it is not necessarily caused by vortex reconnections, whose frequency depends on the vortex line density [21]. To verify that our result is general and does not depend on vortex line density or reconnections, we repeat the calculation in two-dimensional (2D) BECs; such condensates are created when the axial trapping frequency, ω_z, is much greater than the radial trapping one, ω_r, freezing out motion along z. The condensate in the radial plane is also described by Eq. (1), with $C \rightarrow C_{2d} = 2\sqrt{2\pi}aN/a_z$, and $\psi \rightarrow \psi_{2d} = a_r N^{-1/2}\Psi$ which relates the dimensionless wave function to the dimensional 2D condensate wave function, Ψ_{2d}, where $a_r = \sqrt{\hbar/(m\omega_r)}$, $a_z = \sqrt{\hbar/(m\omega_z)}$ denoting the harmonic oscillator lengths in the radial and z directions). To induce turbulence we imprint 42 positive and 42 negative vortices, randomly located and aligned along the axial direction [3]. Here we simulate a 2D ^{23}Na Bose gas with $N = 10^7$ atoms and condensate aspect ratio $\omega_z/\omega_r = 20$ (with $\omega_r = 7.5 \times 2\pi$ Hz), implying $C_{2d} = 8.06 \times 10^4$. The spatial computational domain $|x|, |y| \leq 25$ is discretized on a 1024^2 grid with time step $\Delta t = 10^{-4}$. Choosing our initial monitoring time arbitrarily at $t_0 = 4.4$, we have 86 vortices in the dimensionless condensate area 752, corresponding to a dimensionless vortex line density (number of vortices per unit area) of 0.11. We find a mean radial density $\langle n_{2d}\rangle = 1.23 \times 10^{-4}$, and an estimated healing length $\xi_{2d} = (2C_{2d}n_{2d})^{-1/2} = 0.225$. Proceeding as in 3D, the velocity PDFs and gPDFs of the 2D condensate are shown in Fig. 3 for $\gamma = 0$; we find again nonclassical (non-Gaussian) velocity statistics PDF(v_i) $\propto v_i^b$ with $b = -3.4$ and -3.2 for positive v_x and v_y. These PDFs lack the small wiggles close to zero velocity observed in 3D, as the initial condition induces a more isotropic turbulent state. Unlike the 3D case, in this calculation vortex reconnections play a negligible role, because the number of vortices remains approximately the same. Changing the condensate's radius from 15.5 to 8.9 does not affect the nature of the PDF.

To further confirm the universality of our result, we calculate velocity PDFs in two uniform periodic systems: the first is a homogeneous 3D condensate, which obeys the GPE without the trapping potential; a very isotropic tangle of vortices is produced starting from a spatially random phase [22] on a 128^3 grid and velocity PDFs are computed during the decay. The second is a 2D system of 50 positive and 50 negative coreless vortex points (Onsager vortex gas [23]) which do not reconnect. We find that the PDFs are non-Gaussian in both cases [24] (see Fig. 2 bottom left and right).

We have thus shown (under realistic experimental conditions) how phase imprinting of a staggered array of straight nonintersecting vortices can be used to study quantum turbulence in atomic BECs. We have also found that the decay of turbulence is faster in the presence of a thermal cloud, which we have modeled in a simple way. Our main result is that the statistics of the turbulent superfluid velocity components are non-Gaussian, and, unlike ordinary turbulence, exhibit power-law tails similar to what has been recently measured in turbulent superfluid ^{4}He [11]. Finding velocity statistics similar to ^{4}He in these relatively small systems means that atomic BECs can be used to study quantum turbulence, despite the huge difference in the ratio of intervortex spacing to vortex core radius in atomic BECs (≈ 3 here) and in ^{4}He (10^5 to 10^6). We confirm our 3D result by repeating the calculation in 2D trapped condensates with a different number of vortices and dimensionless vortex line density, and essentially no vortex reconnections, and in two uniform periodic systems: 3D homogeneous condensates and 2D gases of vortex points.

Finally, what is the reason for the observed power-law tails? Clearly vortex reconnection induce high-velocity

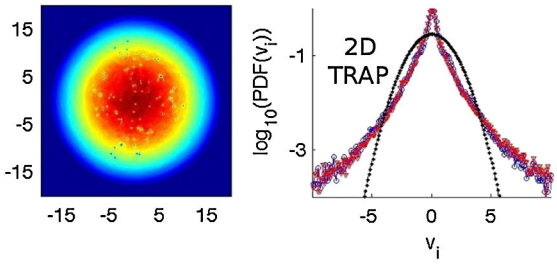

FIG. 3 (color online). Density (left) and velocity PDFs (right) for a trapped 2D BEC ($t_0 = 4.4$, $\gamma = 0$). The maximum density is $n = 2.06 \times 10^{-3}$. Left: 86 vortices (core radius ≈ 2.66) can be identified. Right: Plots of $\log_{10}$[PDF(v_i)] and corresponding $\log_{10}$[gPDF(v_i)] vs v_i, where the v_x, v_y velocity components (sampled within the condensate edge) are blue circles (○) and red triangles (▽); the corresponding gPDF's are black dotted and dash-dotted lines.

events [11], but the simplest explanation is contained in an apparently unrelated study of Min *et al.* [25] of vortex-filament and vortex-blob methods (computational techniques alternative to the direct solution of the Navier-Stokes equations of classical fluid mechanics) who showed that velocity statistics of singular and non singular vortices are qualitatively different. For singular vortices, $\mathrm{PDF}(v_i) \propto v_i^{-3}$ for an isolated vortex; for N vortices, provided that the velocity contribution of each vortex can be considered an independent random variable, the PDF converges to Gaussian but extremely slowly: for example $N \sim 10^6$ vortices (which is much larger than $N \sim 10^2$ of typical BEC experiments) still produces significant tails [26]. Since quantum fluids are characterized by singular vortex cores, Ref. [25] explains the non-Gaussian PDFs observed in the experiment [11] and in our calculations. Indeed, we have directly verified the transition from power law to Gaussian by artificially increasing the core [24] of the classical point vortices. We have also found that in our 2D atomic condensates the correlation function $Q_{xx} = \langle v_x(\mathbf{x}) v_x(\mathbf{x} + r\hat{\mathbf{x}})\rangle / \langle v_x^2 \rangle$ (and similarly for Q_{yy}, where $\langle\cdot\rangle$ means average over $\mathbf{x}$) decays over a distance r of the order of the intervortex spacing, but a weak 10% correlation remains for larger r [24], consistently with [25]. The small value of N is the most likely cause of the failure to converge to Gaussian in small atomic condensates; in larger systems such as turbulent superfluid helium the observed Kolmogorov spectrum [7] implies correlation and organization over many scales and should play the main role in preventing a normal distribution. The intermediate regime poses an interesting problem both for theory and experiments.

We conclude that, due to the singular nature of quantized vorticity and the strict $1/r$ velocity field, the statistics of velocity components are macroscopic observables which distinguish between classical and quantum turbulence. It is worth remarking [27] that for the same reason another such observable is the pressure spectrum, which, in 3D quantum turbulence, should obey a k^{-2} law (where k is the magnitude of the wave vector) rather than the $k^{-7/3}$ scaling which corresponds to the classical Kolmogorov $k^{-5/3}$ spectrum of the energy.

This research was supported by EPSRC and by the Merit Allocation Scheme of the Australian NCI Facility.

*ang.c.white@gmail.com

[1] P. M. Walmsley and A. I. Golov, Phys. Rev. Lett. **100**, 245301 (2008).
[2] D. I. Bradley *et al.*, Phys. Rev. Lett. **101**, 065302 (2008); V. B. Eltsov *et al.*, Phys. Rev. Lett. **99**, 265301 (2007).
[3] T. L. Horng *et al.*, Phys. Rev. A **77**, 063625 (2008).
[4] K. Kasamatsu and M. Tsubota, in *Progress in Low Temperature Physics*, edited by W. P. Halperin and M. Tsubota (Elsevier, Amsterdam, 2009), Vol. XVI, p. 351.
[5] E. A. Henn *et al.*, Phys. Rev. Lett. **103**, 045301 (2009).
[6] W. F. Vinen and J. J. Niemela, J. Low Temp. Phys. **128**, 167 (2002); C. F. Barenghi, Physica (Amsterdam) **237D**, 2195 (2008).
[7] J. Maurer and P. Tabeling, Europhys. Lett. **43**, 29 (1998); C. Nore *et al.*, Phys. Rev. Lett. **78**, 3896 (1997); T. Araki *et al.*, Phys. Rev. Lett. **89**, 145301 (2002); M. Kobayashi and M. Tsubota, Phys. Rev. Lett. **94**, 065302 (2005).
[8] M. R. Smith *et al.*, Phys. Rev. Lett. **71**, 2583 (1993); C. F. Barenghi and L. Skrbek, J. Low Temp. Phys. **146**, 5 (2007).
[9] P. L. Walstrom *et al.*, Cryogenics **28**, 101 (1988).
[10] M. R. Smith *et al.*, Phys. Fluids **11**, 751 (1999).
[11] M. S. Paoletti *et al.*, Phys. Rev. Lett. **101**, 154501 (2008).
[12] A. Vincent and M. Meneguzzi, J. Fluid Mech. **225**, 1 (1991); A. Noullez *et al.*, J. Fluid Mech. **339**, 287 (1997); T. Gotoh *et al.*, Phys. Fluids **14**, 1065 (2002).
[13] S. Burger *et al.*, Phys. Rev. Lett. **83**, 5198 (1999); A. E. Leanhardt *et al.*, Phys. Rev. Lett. **89**, 190403 (2002).
[14] N. G. Berloff and B. V. Svistunov, Phys. Rev. A **66**, 013603 (2002); M. Kobayashi and M. Tsubota, Phys. Rev. A **76**, 045603 (2007); M. Kobayashi and M. Tsubota, J. Low Temp. Phys. **150**, 587 (2008).
[15] N. G. Parker and C. S. Adams, Phys. Rev. Lett. **95**, 145301 (2005).
[16] S. Choi *et al.*, Phys. Rev. A **57**, 4057 (1998); E. J. M. Madarassy and C. F. Barenghi, J. Low Temp. Phys. **152**, 122 (2008); M. Tsubota *et al.*, Phys. Rev. A **65**, 023603 (2002).
[17] A. A. Penckwitt *et al.*, Phys. Rev. Lett. **89**, 260402 (2002); N. P. Proukakis and B. Jackson, J. Phys. B **41**, 203002 (2008).
[18] Refer to http://www.xmds.org for a detailed description.
[19] C. F. Barenghi *et al.*, J. Low Temp. Phys. **138**, 629 (2005); M. Leadbeater *et al.*, Phys. Rev. A **67**, 015601 (2003).
[20] P. Mason, Ph.D. thesis, Cambridge University, 2009.
[21] C. F. Barenghi and D. C. Samuels, J. Low Temp. Phys. **136**, 281 (2004).
[22] N. G. Berloff and A. J. Youd, Phys. Rev. Lett. **99**, 145301 (2007).
[23] S. Wang *et al.*, J. Low Temp. Phys. **149**, 65 (2007).
[24] A. C. White *et al.* (unpublished).
[25] I. A. Min *et al.*, Phys. Fluids **8**, 1169 (1996).
[26] J. B. Weiss *et al.*, Phys. Fluids **10**, 1929 (1998).
[27] D. Kivotides *et al.*, Phys. Rev. Lett. **87**, 275302 (2001).